Hindawi
International Journal of Aerospace Engineering
Volume 2024, Article ID 5569229, 11 pages
https://doi.org/10.1155/2024/5569229

Research Article

Impact Analysis of Different Trajectory Shapes on Optimization Based on Original Natural Algorithm

Yijing Chen, Ying Nan, and Zhihan Li

College of Astronautics, Nanjing University of Aeronautics and Astronautics, Nanjing, Jiangsu, China

Correspondence should be addressed to Yijing Chen; bx1815306@nuaa.edu.cn

Received 10 August 2023; Revised 4 January 2024; Accepted 31 January 2024; Published 20 March 2024

Academic Editor: Guillermo Valencia-Palomo

In this paper, the reentry phase of the Aerospaceplane is taken as the research object, and the performance parameters of the reusable rocket of a private company are analyzed. Aiming at the guidance and control scheme of the spacecraft returning to the reentry trajectory in the real environment, the original natural algorithm is optimized by considering various reentry flight constraints, and the improved original natural algorithm is used to optimize the reentry trajectory of the Aerospaceplane. We obtained two types of reentry trajectories in the presence of large flight-restricted areas, the "S-type" trajectory and the "spiral-type" trajectory, and obtained data on various influencing factors. The results showed that the basic state parameters of the spiral trajectory optimized using the improved original natural algorithm after adding constraints met the constraint conditions. The aerodynamic heating rate and overload of the spiral reentry trajectory were to some extent greater than those of the S-type trajectory. Under the increasingly stringent requirements of the aerospace environment, new requirements were put forward for the thermal protection system to meet the wider environmental situation. This paper uses the improved original natural algorithm for the first time and applies it to the field of aerospace reentry and entry and adds more constraints to this algorithm for computation. Besides, for the first time, the macroscopic nature of trajectory types is used as a comparative element for parameter comparison, providing a reference basis for selecting trajectory optimization directions from the macroscopic perspective of trajectory types.

1. Introduction

In traditional aerospace research, due to the complexity and difficulty of space activities, other matters and engineering will give way to space activities and strive to give space missions greater freedom in the implementation process, in order to successfully complete space missions as much as possible [1–3]. With the development of the times, space missions are no longer limited to this but require more mission requirements. These tasks require more and stricter constraints in scientific research [4, 5].

The reentry and entry of spacecraft refer to the reentry of spacecraft into the Earth's atmosphere or entry the atmospheres of other planets while navigating in space. The optimization of reentry and entry trajectories for spacecraft refers to the optimization of the trajectory from reentering or entering into the atmosphere to the 20 km above the ground. Find the optimal feasible trajectory for this segment of the route based on constraints and objectives. In the past research on reentry trajectory optimization, there was little research and comparison on reentry trajectory shape. Generally, a specific trajectory type was directly analyzed [6]. With the development of space technology, restrictions and constraints increased [7]. The reentry trajectory cannot achieve the target position in the case of a flight exclusion zone. While optimizing the reentry trajectory [8], it is also necessary to classify the trajectory. Therefore, research on the impact of the shape of the reentry trajectory on the reentry situation should be put on the agenda.

The space shuttle emerged during the US-Soviet era, with its fundamental goal being to build a reusable space vehicle that can navigate both inside and outside the atmosphere [9–11]. But in the end, it withdrew from the historical stage due to its safety and economy. The retirement of space

shuttle does not mean that people all over the world stop the research on reusable spacecraft with both aviation and aerospace capabilities. In order to find an economical and safe space shuttle or system, Britain, the United States, Germany, France, Japan, and other countries have launched reusable space shuttle transportation system schemes, and Aerospaceplane research has quietly emerged [12–15]. It is generally believed that the main difference between the Aerospaceplane and the space shuttle is that the space shuttle is an aircraft that takes off vertically like a rocket and lands horizontally like a plane. The Aerospaceplane is a horizontal takeoff and landing aircraft, which enters space orbit by providing power in the atmosphere. The Aerospaceplane is more like a development of the space shuttle, a new thing generated from quantitative change to qualitative change. This paper believes that Aerospaceplane is the future development direction, so this paper selects Aerospaceplane as the research object.

In terms of trajectory optimization, a large number of optimization algorithms have evolved over the past thirty years based on different target requirements. Saraf et al. [16, 17] combined trajectory planning algorithms with trajectory tracking laws to obtain an improved entry acceleration guidance law (EAGLE). On the basis of the reduced order model, drag and lateral acceleration profiles are generated, and three-dimensional trajectories are planned to enable guidance methods to handle reentry guidance problems with strong maneuverability. This method reduces trajectory tracking errors by quickly reconstructing reentry trajectories online. It is a real-time guidance method with the ability of airborne computers to generate reference trajectories, while also considering the feasibility of trajectory design. Xiao et al. discussed the collaborative mechanism for multi-agent-based multisensor collaborative planning technology and explored preliminary research ideas for various key technologies in aerospace operations. However, specific methods still need to be studied [18], and the use of AI's black box problem in the aerospace field still needs to be discussed; Li and Jiang [19] focused on the gliding reentry problem of hypersonic aircraft. Using arc length as the independent variable, they transformed various process constraints into linear constraints. After multiple convex treatments and using the idea of cutting planes to handle the flight-restricted area constraints, they effectively solved the original trajectory planning problem. Sushnigdha utilized the search space reduction (SSR) technique to solve the spacecraft entry trajectory optimization problem. The maximum span was optimized and the minimum heating rate was found, without considering the actual application scenario of the maximum span [20]; Algorithms such as sparrow search algorithm focus on robustness when optimizing design [21] but still remain at the level of unilateral optimization. In order to meet the multicoupling requirements of high real time, uncertainty, robustness, and constraint complexity, better algorithms are needed to achieve trajectory design [22–24]. However, the offline computing power resources on airborne computers are limited and cannot carry a large number of variables in composite computing situations [25]. The enumeration is the fundamental theoretical method for various numerical calculations, but it is not commonly used due to its large computational complexity. Scholars from all walks of life are also using the enumeration to create new numerical algorithms by limiting computational complexity. Casel et al. studied the single-source shortest distance (SSSD) and all pair shortest distance (APSD) problems as enumeration problems, demonstrating that an enumeration point of view can reveal about the problems SSSD and APSD [26]. The original natural algorithm proposed by Nan et al. [27–29] is an exhaustive class algorithm that modifies the dynamic programming method. It considers finding the global optimal solution and searches within a feasible range through a global search of the starting point, saving computational space to a certain extent. The improved original natural algorithm based on computing power space is an exhaustive class algorithm that changes the current computational space used according to the storage space, providing computational results that meet as many requirements as possible within a limited storage space. At the same time, the onboard sensors of the spacecraft obtain information in real time, and the obtained path is replanned after real-time computing of this algorithm. By applying real-time feedback to existing variables for iteration, an improved intelligent adaptive primitive natural algorithm is obtained and applied to trajectory optimization of spacecraft.

This article will use an improved original natural algorithm to optimize two types of reentry trajectories, the first being an "S-type" reentry trajectory and the second being a "spiral" reentry trajectory. In the study of reentry trajectory optimization, S-type reentry trajectories are relatively common. Generally, in a certain perspective, the entry trajectory is an S-type trajectory or a straight line trajectory. This trajectory causes the spacecraft to receive high heat on both sides alternately, or the difference in heat on both sides is not significant, which can reduce the requirements for the spacecraft's thermal protection system. However, the "S-type" trajectory passes through a longer airspace, and in traditional space missions, other tasks give way to successfully completing space missions. Therefore, this did not become a disadvantage of the "S-type" trajectory before. However, with the development of technology in various countries, the requirements for space missions are becoming higher and higher, and the flying area is beginning to be limited. We have also begun to study flight trajectories that meet higher requirements.

The main innovations and contributions of this paper are as follows:

(1) The original natural algorithm has been applied to the field of aerospace reentry and entry for the first time, and more constraints have been added to this algorithm for computation, achieving more precise trajectory optimization design calculations

(2) For the first time, the macroscopic nature of trajectory types is used as a comparative element for parameter comparison, providing a reference basis for selecting trajectory optimization directions from the macroscopic perspective of trajectory types

2. Problem Description

The optimization problem of reentry trajectory for spacecraft entry and return is defined as the trajectory optimization problem during the flight process from the beginning of spacecraft entry into the atmosphere to just before landing. Specifically, this study focuses on the design and optimization of flight trajectories from altitudes of 120 km to around 20 km. The reentry process is a deceleration process, from a high-speed deceleration in the orbit to a safe landing speed near the surface. Generally, there are two methods for reentry, using retro-rocket to decelerate and using aerodynamic forces to decelerate, but both methods can also be used simultaneously. This article focuses on decelerating the spacecraft without the use of retro-rocket, solely utilizing the resistance of the dense atmosphere to the spacecraft, that is, using aerodynamic forces to decelerate the spacecraft and optimizing its trajectory to make it safe, economical, and feasible.

This issue is subject to the following assumption of constraints:

(1) Equality constraint

(2) Inequality constraint

(3) Boundary condition constraints

(4) Flight exclusion zone constraints (obstacle avoidance constraints)

2.1. Equation Constraints. Considering the six degrees of freedom variables of the Aerospaceplane during reentry flight, the reentry process is modeled, and the differential motion equation is obtained:

$$\dot{V} = \frac{P\cos\alpha\cos\beta - c_x qS}{m} - g\sin\gamma + \omega_d^2 r\cos\phi(\sin\gamma\cos\phi - \cos\gamma\sin\psi\sin\phi) + a_{Wx}, \tag{1}$$

$$\dot{\gamma} = \frac{P(\sin\alpha\cos\sigma + \cos\alpha\sin\beta\sin\sigma)}{mV} + \frac{c_y qS\cos\sigma}{mV} - \frac{c_x qS\sin\sigma}{mV} + \omega_d^2 r\cos\phi\frac{\cos\gamma\cos\phi + \sin\gamma\sin\psi\sin\phi}{V} + \left(\frac{V}{r} - \frac{g}{V}\right)\cos\gamma + 2\omega_d\cos\psi\cos\phi + \frac{a_{Wy}}{V}, \tag{2}$$

$$\dot{\psi} = \frac{P(\sin\alpha\cos\sigma + \cos\alpha\sin\beta\cos\sigma)}{mV} - \frac{qS}{mV\cos\gamma}(C_y\sin\sigma + C_z\cos\sigma) + 2\omega_d(tg\gamma\sin\psi\cos\phi - \sin\phi) - \frac{\omega_d^2 r}{V\cos\gamma}\cos\psi\sin\phi\cos\phi - \frac{V}{r}\cos\gamma\cos\psi tg\phi + \frac{a_{Wz}}{V\cos\gamma}, \tag{3}$$

$$\dot{h} = V\sin\gamma + V_{Wy}, \tag{4}$$

$$\dot{\theta} = V\cos\gamma\cos\psi + V_{Wx}, \tag{5}$$

$$\dot{\phi} = -V\cos\gamma\sin\psi + V_{Wz}. \tag{6}$$

In the above equations V, γ, and ψ, respectively, represent the speed, trajectory inclination angle, and yaw angle of the reentry vehicle; α, β, and σ are the corresponding angle of attack, sideslip angle, and roll angle; S and L, respectively, are the reference area and reference length; C_x, C_y, and C_z are the drag coefficient, lift coefficient, and side force coefficient; h, θ, and φ are the distance between the altitude, longitude, and latitude of the spacecraft; P is the engine thrust; V_{W_y}, V_{W_x}, and V_{W_z} are the wind speeds in the vertical, longitude, and latitude directions of the spacecraft's in the ground coordinate system; a_{W_y}, a_{W_x}, and a_{W_z} are the wind shear in y-, x-, and z-directions in the ballistic coordinate system; R is the Earth radius; g_0 is the gravitational acceleration at sea level.

The six degrees of freedom equations of motion used in this paper include the wind field term, wind shear, for two reasons: first, with the improvement of reentry accuracy requirements, more influencing factors should be considered. The second is that when the spacecraft enters other planets with high wind field magnitude, the influence of wind field must be considered.

The following is the resistance of spacecraft during aerodynamic deceleration reentry into the atmosphere, D:

$$D = \frac{1}{2}\rho V^2 C_D S. \tag{7}$$

Among them, ρ is the density of air of the current position, S is the cross-sectional area of the spacecraft, and C_D is the drag coefficient.

2.2. Inequality Constraint. Due to the material and performance limitations of various parts of the spacecraft, the corresponding indicators of each onboard equipment are required to not exceed the upper limit. Then, compare and take the minimum upper limit requirement. During the flight process, there are requirements for aerodynamic heating, overload, dynamic pressure, and other indicators, creating intangible flight-restricted areas. The airspace that meets the requirements is the reentry corridor. The constraints for reentry corridors include the following:

Aeroheating rate

$$\dot{Q}_S(t) \le \dot{Q}_{S\mathrm{Max}}. \tag{8}$$

Overload

$$n_Y(t) \le n_{Y\mathrm{Max}}. \tag{9}$$

Dynamic pressure

$$q(t) \le q_{\mathrm{Max}}. \tag{10}$$

Control parameters

$$u_{i,\min} \le u_i(t) \le u_{i,\max}. \tag{11}$$

The following is the calculation formula for surface temperature of reentry aircraft:

$$T_w = \left(\frac{\dot{Q}}{\varepsilon\sigma}\right)^{0.25}. \tag{12}$$

Among them, ε is the radiant emissivity of the surface material, $\varepsilon = 0.8$; $\sigma = 5.6685 \times 10^{-3}$ J/m^{2}K^4 sec is the Boltzmann constant.

2.3. Boundary Condition Constraints. The constraints of boundary conditions come from the requirements of the research topic, defining the starting and ending conditions. This constraint is expressed as follows:

$$\begin{aligned} V(t_0) &= V_0, \\ \gamma(t_0) &= \gamma_0, \\ \psi(t_0) &= \psi_0, \\ \theta(t_0) &= \theta_0, \\ h(t_0) &= h_0, \\ \phi(t_0) &= \phi_0, \\ V(t_f) &= V_f, \\ \gamma(t_f) &= \gamma_f, \\ \psi(t_f) &= \psi_f, \\ \theta(t_f) &= \theta_f, \\ h(t_f) &= h_f, \\ \phi(t_f) &= \phi_f. \end{aligned} \tag{13}$$

Among them, $V(t_0)$, $\gamma(t_0)$, $\psi(t_0)$, $\theta(t_0)$, $h(t_0)$, $\phi(t_0)$ are the six state variables at the starting point, which are velocity, trajectory inclination, yaw angle, latitude, altitude, and accuracy.

2.4. Flight Exclusion Zone Constraints. Space constraint refers to the prohibited flight zones that spacecraft should avoid in the airspace and the areas that must be passed through according to the requirements of the space mission objectives. The mathematical expression for the 3D flight-restricted area is

$$\vec{X}(x, y, z) \notin A_{\text{Threat},i}(x, y, z, t, \cdots), i = 1, 2, \cdots, N_{\text{AT}}. \tag{14}$$

In the above equation, $\vec{X}(x, y, z)$ is the flight trajectory parameter vector, (x, y, z) is the coordinates in 3D space, and $A_{\text{Threat},i}$ is the i-th 3D restricted zone. There are a total of N_{AT} 3D flight-restricted zones. The 3D flight exclusion zone can vary over time and under certain conditions.

The following is the mathematical expression of task points:

$$\vec{X}(x, y, z) \in A_{\text{Waypoint},i}(x, y, z, t, \cdots), i = 1, 2, \cdots, N_{\text{Wp}}. \tag{15}$$

In the above equation, $A_{\text{Waypoint},i}$ is the i-th 3D task point space, with a total of N_{Wp} 3D task points that can change over time and under certain conditions.

3. Solving of Trajectory Optimization Algorithm

During the reentry flight process, data search and feedback are required to obtain the globally optimal reentry flight trajectory. A large number of existing algorithms have chosen specific algorithms for a certain problem [30], but reentry is a consistent process that requires comprehensive consideration of various factors. This chapter applies the theory of original natural algorithms to the reentry of spacecraft, achieving global minimization of M performance indicators. In subsequent research, it is possible to consider more subsystems, add all available performance indicators, and optimize them to cope with more complex atmospheric and airspace environments.

3.1. Global Optimization of Indicators. During the specified reentry flight process, M performance indicators are minimized globally. In this article, we consider optimizing $M = 6$ performance indicators simultaneously:

$$J = \min_{U(t)\in\Omega_U} \begin{bmatrix} J_1(t) \\ J_2(t) \\ \cdots \\ J_6(t) \end{bmatrix}. \tag{16}$$

In the equation, the optimized performance indicators include the following: $J_1(t)$ is the total aerodynamic heating amount Q_S, $J_2(t)$ is the maximum aerodynamic heating rate $\dot{Q}_{S\text{Max}}$, $J_3(t)$ is the total dynamic pressure q_S, $J_4(t)$ is the maximum dynamic pressure q_{Max}, $J_5(t)$ is the total overload n_S, and $J_6(t)$ is the maximum overload n_{Max}. Among them,

$$\begin{cases} Q_S = \displaystyle\int_{t_0}^{t_f} \dot{Q}_S(t)dt, \\ \dot{Q}_S(t) = \dfrac{17600}{\sqrt{R_N}}\sqrt{\dfrac{\rho}{\rho_0}}\left(\dfrac{V}{V_0}\right)^{3.15}, \end{cases} \tag{17}$$

Table 1: Simulation starting point parameters.

Aerospaceplane	Spiral-type trajectory 1	Spiral-type trajectory 2	S-type trajectory
x-axis (km)	-1138	737.7	-2050
y-axis (km)	120.1	120	120.2
z-axis (km)	1302	550	1296
Velocity (m/s)	7800	7800	7800
Path angle (°)	-2.5	-2.5	-2.5
Yaw angle (°)	-6.01101e-6	179.922	239.896

where R_N is the radius of the stationary point of the nose cone.

$$\begin{aligned} q_S &= \int_{t_0}^{t_f} q(t)dt, \\ q(t) &= 0.5\rho V^2, \\ n_S &= \int_{t_0}^{t_f} n_y(t)dt, \\ n_y(t) &= \frac{a_y}{g}. \end{aligned} \tag{18}$$

Among them, t is the time, t_0 and t_f are the initial and terminal moments of spacecraft reentry, respectively, V is the velocity of the spacecraft, ρ and ρ_0 are the atmospheric density at the altitude of the aircraft and the atmospheric density at sea level, g is the gravitational acceleration of the aircraft location, and a_y is the acceleration in the y-direction.

The stochastic control system can also be described by the nonlinear time-varying dynamic differential equations (1)–(6) as follows:

$$\frac{dx(t)}{dt} = f[t, \mathbf{X}(t), \mathbf{U}(t), w(t), p]. \tag{19}$$

In the above equation, t is the time, $t \in [t_0, t_f]$; $\mathbf{X}$ is the status parameter, $\mathbf{X} = [V, \gamma, \psi, h, \theta, \phi]$; $\mathbf{U} = [\alpha, \sigma]$ is the control parameter; w is the random interference term; p is a static parameter that does not change over time; and f describes the dynamic system function affected by other variable parameters.

3.2. Definition and Related Deductions of Subsystems. Subsystems refer to each functional module in a large spacecraft system, and each subsystem includes indicators of the items it needs to meet. In the idea of the original natural algorithm, the indicators of each dimension of all subsystems will be optimized. The indicators that need to be optimized include optimality, robustness, adaptability, and fault tolerance.

Initial operating state parameters of the subsystem:

$$x_i(t_{i0}) = x_{i0}, u_i(t_{i0}) = u_{i0}. \tag{20}$$

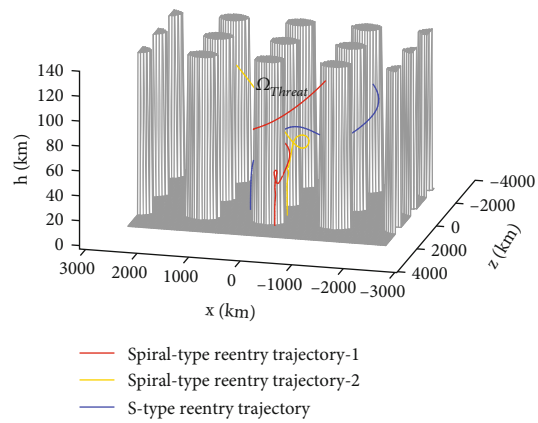

Figure 1: 3D diagram of three reentry trajectories with the forbidden area.

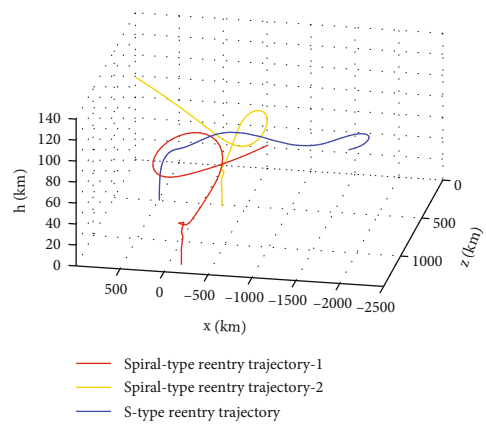

Figure 2: 3D diagram of three reentry trajectories without display of the restricted area.

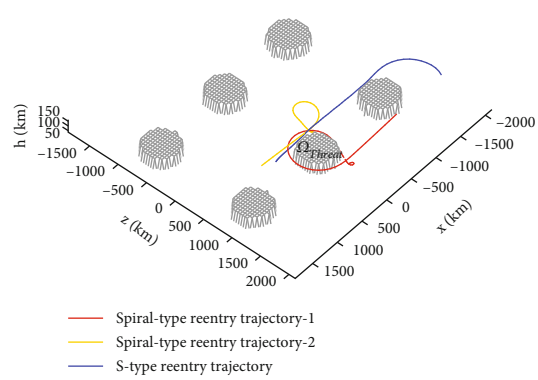

Figure 3: 3D diagram of three flight trajectories approaching top view angle.

Terminal state parameters of subsystems:

$$x_i(t_{if}) = x_{if}. \tag{21}$$

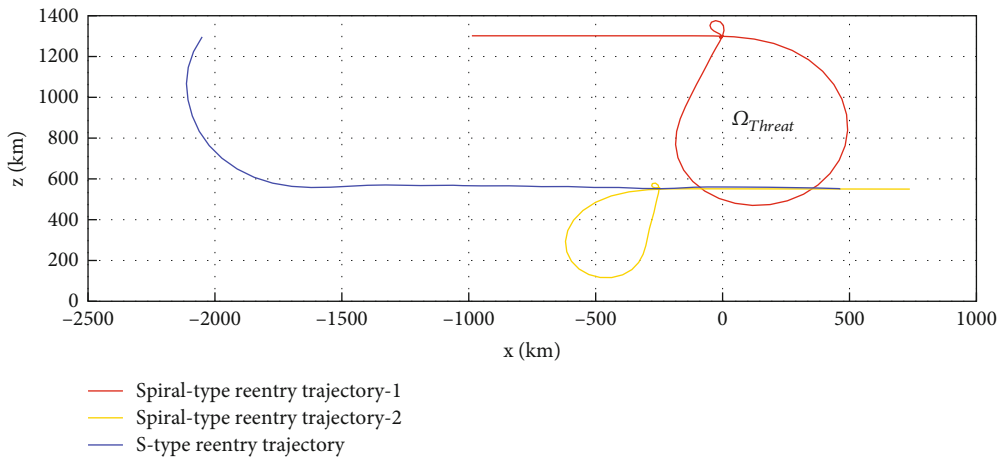

Figure 4: Top view of three flight trajectories of Aerospaceplane.

Table 2: Coordinates of key points for three reentry trajectories.

x-axis endpoint coordinates	Spiral-type trajectory 1	Spiral-type trajectory 2	S-type trajectory
Negative direction (km)	(-987.7, 1302)	(-619, 293.7)	(-2112, 1067)
Positive direction (km)	(492.7, 838.6)	(737.7, 550)	(461.7, 550.2)
Span in x-axis direction (km)	1480.4	1356.7	2573.7

Subsystem process constraints:

$$g_{i,\mathrm{Min}} \le g_i(t, \mathbf{X}, \mathbf{U}, \mathbf{W}) \le g_{i,\mathrm{Max}}. \tag{22}$$

In the above equation, g_i is a vector of size n_{gi}, and each subsystem has different values; $\mathbf{W}$ refers to external interference, $\mathbf{W} = [w_1, w_2, \cdots, w_s]$. The constraints on control parameters $u_i(t)$ and $P_i(t)$ are as follows:

$$u_{i,\mathrm{Min}} \le u_i(t) \le u_{i,\mathrm{Max}}, \tag{23}$$

$$P_{i,\mathrm{Min}} \le P_i(t) \le P_{i,\mathrm{Max}}. \tag{24}$$

The random interference model in each subsystem is shown by the following differential equation:

$$\frac{dw_i(t)}{dt} = h[t, w_i(t), v_i(t), x_i(t)], i = 1, 2, \cdots, 6, \tag{25}$$

where h describes the differential relationship between random disturbances, state variables, and expected control. $v_i(t)$ is the expected control variable for random disturbance $w_i(t)$.

During flight process, each subsystem is set to have the following performance indicators:

$$J_{i,j}[u_i(t)] = \int_{t_{i0}}^{t_{\mathrm{if}}} L_{i,j}[t, X(t), u_i(t), w_i(t), p_i]dt, i = 1, 2, \cdots, T. \tag{26}$$

In the equation, $[t_{i0}, t_{\mathrm{if}}]$ represents the time period during which subsystem i operates during flight. Terminal constraints are expressed as performance indicators:

$$J_{i,T+1}[u_i(t)] = \Phi_i[x_i(t_{\mathrm{if}}), t_{\mathrm{if}}]. \tag{27}$$

Among them, $\Phi_i[x_i(t_{\mathrm{if}}), t_{\mathrm{if}}]$ is the terminal cost.

The optimal control problem is to find the optimal input control parameters $U^*(t) = [u_1^*(t), u_2^*(t), \cdots, u_S^*(t)]$ of the S subsystem that is randomly perturbed during the i-th time period. Large-scale stochastic control systems start from initial condition (Eq. (20)) to terminal conditions (Eq. (21)) and make multiple performance indicators achieve global minimization along the trajectory under inequality constraints (Eqs. (22)–(24)).

$$\min J_{U(t)\in\Omega_U} = \min \begin{bmatrix} J^1_{U_1(t)} \\ J^2_{U_2(t)} \\ \cdots \\ J^S_{U_S(t)} \end{bmatrix} == \min \begin{bmatrix} J_{1,1}, J_{1,2}, \cdots, J_{1,T+1} \\ u_1(t) \quad u_1(t) \qquad u_1(t) \\ J_{2,1}, J_{2,2}, \cdots, J_{2,T+1} \\ u_2(t) \quad u_2(t) \qquad u_2(t) \\ \cdots \\ J_{S,1}, J_{S,2}, \cdots, J_{S,T+1} \\ u_S(t) \quad u_S(t) \qquad u_S(t) \end{bmatrix}. \tag{28}$$

The constraints include initial trajectory inclination angle of reentry point, maximum aerodynamic heating rate, maximum overload, and landing point position. The optimization conditions include pneumatic heating capacity, pneumatic heating rate, dynamic pressure, and overload. If certain performance indicators need to be maximized, they can be

minimized by assigning corresponding negative values to the corresponding parameters in the matrix of Eq. (28), as shown in mutator (29), and passing them to Eq. (28).

$$-J_{i,j} \longrightarrow J_{i,j}. \tag{29}$$

4. Trajectory Simulation Analysis

4.1. Simulation Scenario Description. The Aerospaceplane conducts reentry flight in an airspace with restricted areas. The destination target is to land near the restricted area Ω_{Threat}, where the distance L_Ω between the terminal coordinate of the aircraft and the vertical line of the center of the section of the restricted area Ω_{Threat} is longer than the radius of the section of the restricted area and less than twice the half diameter of the cross section of the restricted area. The mathematical expression is $250\,\text{km} < L_\Omega < 500\,\text{km}$.

The starting point is located at an altitude of 120 km from the ground, with a starting flight speed of 7800 m/s. The Aerospaceplane is required to avoid the flight-restricted area during flight and land in the landing section within the target area.

In the simulation process, according to different entry points, combined with various parameters of the Aerospaceplane, numerical simulation was carried out through the C++ programming in the WIN10 system, and different reentry trajectory data were obtained through simulation. The basic parameters of the Aerospaceplane mathematical model are set as follows: lift-to-drag ratio $\lambda = 0.35$, aerodynamic reference area $S = 95\,\text{m}^2$, mass $M = 20000\,\text{kg}$, heating rate $\dot{Q}_S \leq \dot{Q}_{S\text{Max}} = 400\,\text{kw/m}^2$, and overload $n_Y \leq \dot{n}_{Y\ \max} = 2\,\text{g}$. The basic parameters of the simulation in this article are model parameters designed based on the parameters of space shuttles developed by various countries. At the same time, this simulation method can be extended to similar spacecraft. This generalizable algorithm is also one of the main objectives of this article: to use only one algorithmic approach to optimize the aerospace reentry trajectory, satisfy various possible constraints and objectives, and obtain the optimal reentry trajectory from a global perspective.

The simulation starting point parameters are shown in Table 1.

4.2. Simulation Result. Many trajectories were obtained through simulation, and three representative trajectories were selected for analysis.

The principle of the original natural algorithm is used for digital programming simulation. In the case of flight span requirements, the simulation results are shown in Figure 1. The red solid line and the yellow solid line are representative of the reentry trajectory with transverse span requirements in the reentry process of Aerospaceplane aircraft, and the blue solid line is representative of the reentry trajectory without transverse span requirements in the reentry process of Aerospaceplane aircraft.

The red solid line represents the spiral-type trajectory 1, the yellow solid line represents the spiral-type trajectory 2, and the blue solid line represents the S-type trajectory.

Figure 2 shows the 3D diagram of three reentry flight paths of Aerospaceplane without displaying the flight-restricted area. In order to more clearly see the spatial relationship of the three trajectories and their relationship with the flight-restricted zone, Figure 3 is presented. Figure 4

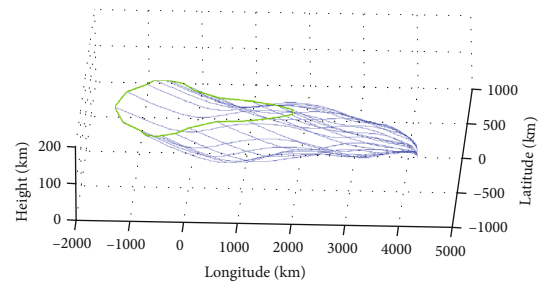

Figure 5: Display of simulation results for a large number of S-type reentry trajectories.

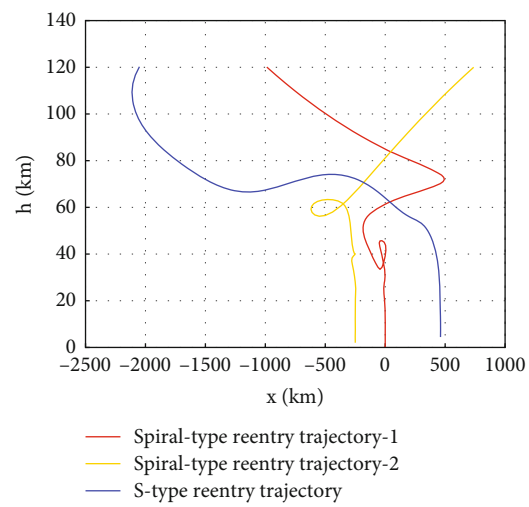

Figure 6: Flight trajectories side view of two types of tracks of Aerospaceplane.

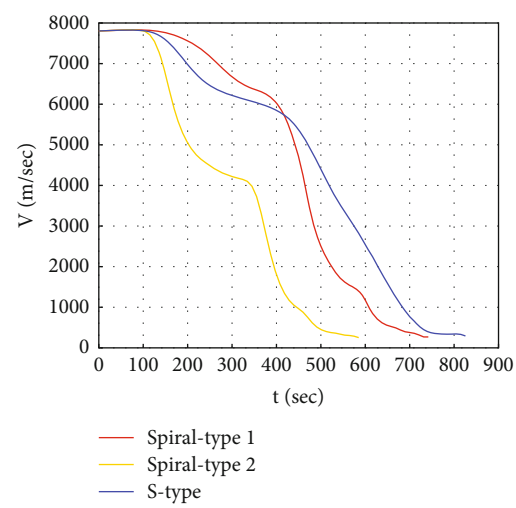

Figure 7: Time-varying curve of speed of two types of trajectories of Aerospaceplane.

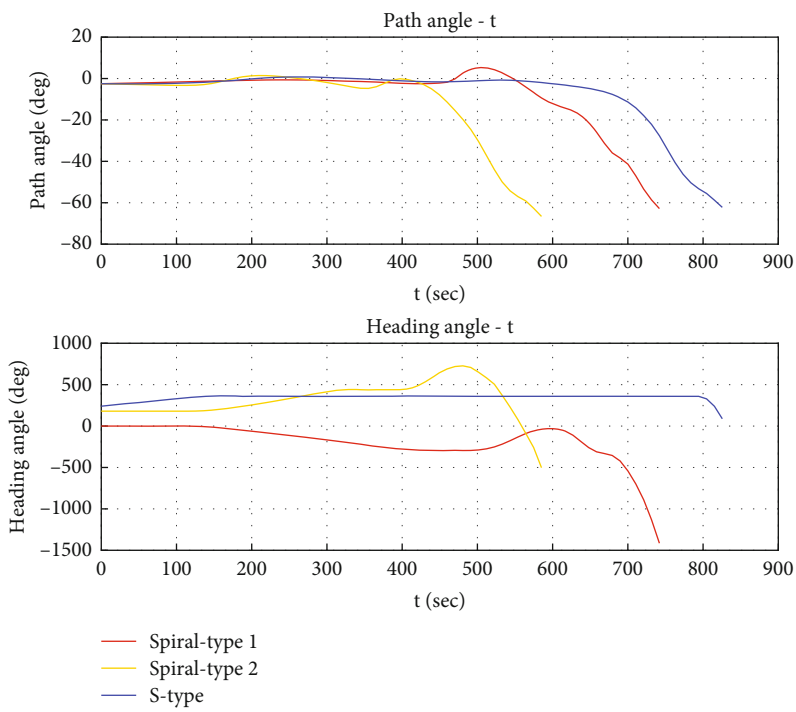

Figure 8: Curve of path angle and heading angle of two types of trajectories of Aerospaceplane with time.

shows a top view of two types of trajectories. From Figures 2 and 3, the characteristics of the three trajectories can be directly observed:

(1) The spiral-type trajectory 1 Aerospaceplane circle the restricted area for reentry flight, occupying less airspace within the allowed airspace

(2) The spiral-type trajectory 2 Aerospaceplane conducts reentry flight between forbidden flight areas, which occupies more allowable airspace than spiral-type trajectory 1

(3) The S-type reentry trajectory does not need to consider the occupation of airspace and only avoids the flight-restricted area. Therefore, the top view can have a straight line or S-type curve shape of the reentry trajectory, which occupies the most airspace

The z-direction spans of the spiral-type reentry trajectory 1 and the S-type reentry trajectory are similar, while the spiral-type reentry trajectory 2 does not need to fly around the restricted area, so the longitudinal span is smaller. The coordinates of some key points on each curve are given in Table 2.

In Figure 5, the blue curve represents the simulated trajectory of a large number of S-type trajectories, with a reentry altitude of 120 km and a reentry point velocity of 7800 m/s. The target endpoint of all trajectories is the same, and the green line represents the starting point of each trajectory. In the reentry trajectories of Figure 5, the maximum horizontal span is about 5500 km, and the minimum horizontal span is about 2400 km. It can also confirm that the S-type reentry trajectory cannot further reduce the horizontal span under the same initial height and speed conditions.

Figure 6 shows the side view curves of three trajectories. Since the outer side of the turning radius of the Aerospaceplane is more severely ablated than the inner side when turning, it can be seen from Figures 1–4 that the S-type reentry trajectory turns in different directions at different positions, so there is no clear difference in the external ablation degree of the Aerospaceplane. However, the spiral reentry trajectory mostly turns in the same direction, so there will be a significant difference in the erosion situation on the inner and outer sides of the turning radius.

Figures 7 and 8 show the variation of Aerospaceplane speed, trajectory inclination, and yaw angle with time. From the simulation results of the selected trajectory, it can be seen that when the flight speed of the Aerospaceplane slows down to below 3000 m/s, the spiral-type reentry trajectory 1 is about 100 s faster than the S-type reentry trajectory. The spiral-type reentry trajectory 2 exhibits deceleration differences 100 seconds after the start of reentry. The energy consumed during deceleration is also reflected in the heat generation level, i.e., the heating rate.

Figure 9 shows the change curve of control quantity of two types of trajectories of Aerospaceplane with time. The control variables include attack angle, roll angle, and acceleration.

Figure 10 shows the relationship between aerodynamic heating rate and time of two trajectories of Aerospaceplane. The unit of heating rate is kilowatts per square meter. It can be clearly seen from the figure that the peak heating rate of spiral reentry trajectory 1 is close to three times that of the peak heating rate of S-type reentry trajectory. The heating

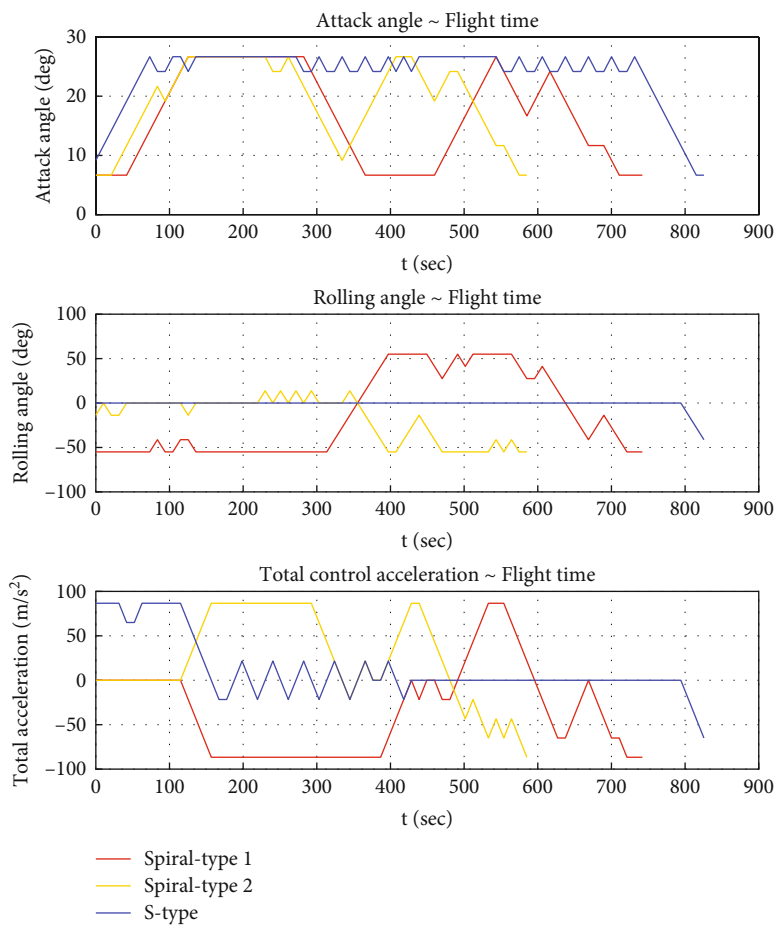

Figure 9: Time-varying curve of control quantities of two types of trajectories of Aerospaceplane.

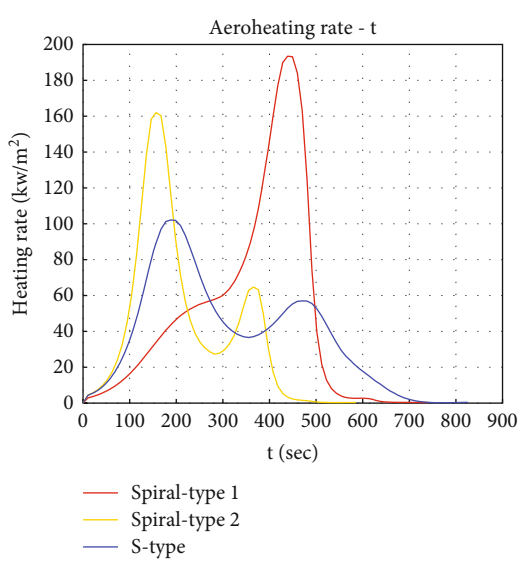

Figure 10: Time-varying curve of heating rate of two types of trajectories of Aerospaceplane.

rate value is the area with the highest heating rate on the Aerospaceplane. The reason for this situation also confirms that there is a significant difference in the erosion of the inner and outer sides of the turning radius mentioned earlier. The reentry phase of a spacecraft is a deceleration process that involves the conversion of potential energy and kinetic energy into thermal energy. The heating rate during the return process is correlated with parameters such as the spacecraft's speed and current air density. Different types of trajectories can lead to different changes in speed and altitude at different stages, so the changes in heating rate will also have different situations at different stages. As shown in Figure 10, when the heating rate of the S-type reentry trajectory is high, the heating rate is reduced by increasing the altitude of the aircraft, which sacrifices the time consumed during the reentry process. From Figure 7, it can be seen that there is only one obvious deceleration interval for the spiral-type reentry trajectory 1, so the heating rate in Figure 10 has only one crest. In Figure 7, it can be seen that the spiral-type reentry trajectory 2 has two steep deceleration regions, so there are two crests of heating rates in Figure 10. So, the maximum heating rate of spiral-type reentry trajectory 1 will be higher than that of S-type reentry trajectory and spiral-type reentry trajectory 2.

Figure 11 shows the relationship between overload and time for two types of reentry trajectories. During the peak overload stage, a small amount of overload exceeds the maximum overload required in this article in a short period of

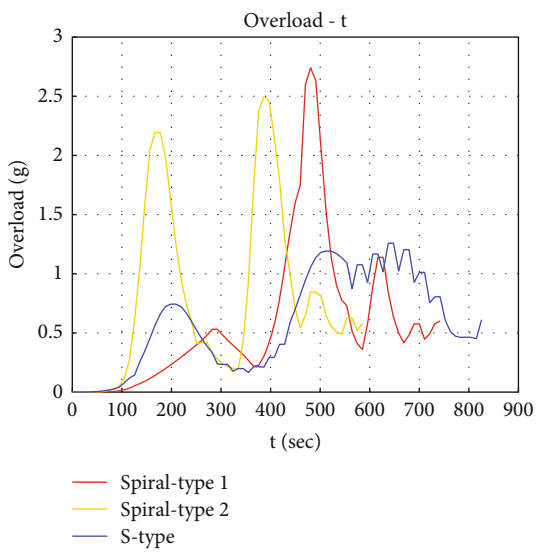

Figure 11: Time-varying curve of overload of two types of trajectories of Aerospaceplane.

time. The time to exceed the constraint overload is very short. If there is a demand, the maximum overload can be reduced in real time by changing the attitude or increasing the active braking force during the overload rise phase. The overall simulation results are within an acceptable range.

5. Conclusion

In the past, there have been almost no restrictions on the use of airspace during the reentry process of space activities. This article groundbreaking unveils the research and analysis of the reentry process under airspace restrictions. Based on the idea of original natural algorithms, it improves the participation method of new constraint requirements and calculates the various parameters of reentry under airspace restrictions for the first time. Research has shown that, in response to constraint requirements, the spiral-type reentry trajectory significantly reduces the range of horizontal airspace usage compared to the general reentry activity, namely, the S-type reentry trajectory. Moreover, after optimization calculation by the improved original natural algorithm, all basic flight parameters are within the acceptable range of constraints.

From the simulation results in this article, it can be seen that the state parameters of both spiral reentry trajectories meet the rationality conditions. The heating rate and overload of the spiral reentry trajectory are greater than those of the S-type reentry trajectory. According to the optimization algorithm in this article, reasonable new requirements for the thermal protection system are proposed based on the target object's situation, while avoiding the flight ban zone and minimizing the horizontal flight airspace. On the other hand, the airspace used can also be calculated based on the limits of the thermal protection system. In practical applications, reverse double helix trajectories can also be attempted to reduce the erosion difference between the inner and outer sides, which requires further research.

The future trajectory optimization calculation will improve with the development of basic technologies such as sensor real-time sensing ability and embedded computer computing ability, and there will be a more refined target demand for trajectory optimization goals. And different types of trajectory analysis will also be applied to reentry and entry in different situations. Flight exclusion zones may include solid terrain flight exclusion zones, administrative flight exclusion zones, and atmospheric motion flight exclusion zones. Specific situations need to be distinguished for different planets, and more targeted research is needed in the future.

Data Availability

The data used to support the findings of this study are available from the corresponding author upon request.

Conflicts of Interest

The authors declare that they have no conflicts of interest.

Acknowledgments

This research was funded by the cooperative project with China Aerospace Science and Technology Corporation (No. FdJX-YY-22-282).

References

[1] T. Rabus, "Safety standards for launch and re-entry operations: overview of current risk management policies in different countries and industries," *Journal of Space Safety Engineering*, vol. 10, no. 3, pp. 331–339, 2023.

[2] E. Suhir, "Chapter 36-Probabilistic reliability-physics models in aerospace human-in-the-loop (HITL) problems," in *DHM and Posturography*, pp. 499–516, Academic Press, 2019.

[3] W. J. Renton, "Aerospace and structures: where are we headed?," *International Journal of Solids and Structures*, vol. 38, no. 19, pp. 3309–3319, 2001.

[4] K. S. Poniatowski and M. G. Osmolovsky, "Capabilities, costs, and constraints of space transportation for planetary missions," *Acta Astronautica*, vol. 35, no. 1, pp. 587–596, 1995.

[5] W. Luo, G. Lei, X. Zheng, Y. Li, and C. Lai, "Rapid reentry trajectory planning based on geometric-dynamic method," *Journal of Engineering Research*, vol. 11, no. 3, pp. 227–235, 2023.

[6] H. T. Zhan, W. P. Zhan, and L. Guo, "Simulation on point of fall accuracy for skip re-entry vehicle," in *China Academic Journal Electronic Publishing House, Proceedings of the 15th National Conference on Signal and Intelligent Information Processing and Application*, pp. 51–54, Beijing, China, 2022.

[7] A. Hänel, T. Schnellhardt, E. Wenkler et al., "The development of a digital twin for machining processes for the application in aerospace industry," *Procedia CIRP*, vol. 93, pp. 1399–1404, 2020.

[8] J. L. Zhang, D. P. Zhou, D. P. Yang, R. Liu, and K. Liu, "Computation method for reachable domain of aerospace plane under the influence of no-fly zone," *Acta Aeronautica et Astronautica Sinica*, vol. 42, no. 8, pp. 525771-1–525771-14, 2021.

[9] G. Zuppardi, R. Savino, G. Russo, L. Spano' Cuomo, and E. Petrosino, "Aerodynamic analysis of the aerospaceplane

HyPlane in supersonic rarefied flow," *Acta Astronautica*, vol. 123, pp. 229–238, 2016.

[10] J. Song and H. Q. Su, "The ascent trajectory optimization of two-stage-to-orbit aerospace plane based on pseudospectral method," *Procedia Engineering*, vol. 99, pp. 1044–1048, 2015.

[11] K. H. Kang and L. Fu, "Research on operational application of US military aerospaceplane," *Aerodynamic Missile Journal*, vol. 51, no. 12, pp. 104–110, 2021.

[12] S. Singh, S. Stappert, L. Bussler, M. Sippel, Y. C. Kucukosman, and S. Buckingham, "Full-scale simulation and analysis of formation flight during in-air-capturing of a winged reusable launch vehicle," *Journal of Space Safety Engineering*, vol. 9, no. 4, pp. 541–552, 2022.

[13] B. U. Jo and J. Ahn, "Optimal staging of reusable launch vehicles for minimum life cycle cost," *Aerospace Science and Technology*, vol. 127, article 107703, 2022.

[14] M. Balesdent, L. Brevault, B. Paluch et al., "Multidisciplinary design and optimization of winged architectures for reusable launch vehicles," *Acta Astronautica*, vol. 211, pp. 97–115, 2023.

[15] X. Y. Gu, J. G. Guo, Z. Y. Guo, L. K. Qiu, Y. Zhao, and G. Q. Wang, "Performance improvement-oriented re-entry attitude control for reusable launch vehicles with overload constraint," *ISA Transactions*, vol. 128, no. Part A, pp. 386–396, 2022.

[16] A. Saraf, J. A. Leavitt, D. T. Chen, and K. D. Mease, "Design and evaluation of an acceleration guidance algorithm for entry," *Journal of Spacecraft and Rockets*, vol. 41, no. 6, pp. 986–996, 2004.

[17] J. A. Leavitt and K. D. Mease, "Feasible trajectory generation for atmospheric entry guidance," *ournal of Guidance, Control, and Dynamics*, vol. 30, no. 2, pp. 473–481, 2007.

[18] J. K. Xiao, W. M. Li, and B. Liu, "Analysis of key technologies in mission planning for aerospace defense operations," *Aerodynamic Missile Journal*, vol. 46, no. 2, pp. 51–55, 2015.

[19] J. Li and J. Y. Jiang, "Online trajectory planning algorithm for hypersonic glide re-entry problem," *Journal of Beijing University of Aeronautics and Astronautics*, vol. 46, no. 3, pp. 579–587, 2020.

[20] G. Sushnigdha, "Spacecraft re-entry trajectory optimization using search space reduction technique," *IFAC-PapersOnLine*, vol. 55, no. 1, pp. 46–51, 2022.

[21] H. Xu, G. B. Cai, S. X. Zhang, X. G. Yang, and M. Z. Hou, "Hypersonic re-entry trajectory optimization by using improved sparrow search algorithm and control parametrization method," *Advances in Space Research*, vol. 69, no. 6, pp. 2512–2524, 2022.

[22] Y. Nan, G. Q. Huang, Y. P. Lu, and P. Gong, "Global 4-D trajectory optimization for spacecraft," *Science China Technological Sciences*, vol. 43, no. 6, p. 636, 2010.

[23] Y. Nan, Y. P. Lu, and P. Gong, "Optimal re-entry trajectory design for mooncraft returning to the earth," *Journal of Astronautics*, vol. 30, no. 9, pp. 1842–1847, 2008.

[24] D. P. Bertsekas, "Dynamic programming and suboptimal control: a survey from ADP to MPC∗," *European Journal of Control*, vol. 11, no. 4–5, pp. 310–334, 2005.

[25] N. Sun, Y. Bao, and D. Fan, "The rise of high-throughput computing," *Frontiers of Information Technology & Electronic Engineering*, vol. 19, no. 10, pp. 1245–1250, 2018.

[26] K. Casel, T. Friedrich, S. Neubert, and M. L. Schmid, "Shortest distances as enumeration problem," *Discrete Applied Mathematics*, vol. 342, pp. 89–103, 2024.

[27] Y. Nan, Q. X. Ding, S. D. Chen, G. Q. Huang, and J. Zou, "Integrated global optimization design of multiple aircraft trajectories based on natural numerical algorithms," *Chinese Science: Technical Science*, vol. 43, no. 6, pp. 636–659, 2013.

[28] Y. J. Chen and Y. Nan, "Route planning of multiple aircraft based on natural natural elimination-evolutional optimization algorithm," *Command Information System and Technology*, vol. 12, 2021.

[29] H. X. Chen, J. Wu, F. H. Meng, Q. H. Pan, and Y. Nan, "Trajectory optimization of multi-aircraft confrontation based on improved natural computation," *Chinese Control And Decision Conference (CCDC)*, vol. 32, pp. 432–436, 2020.

[30] G. Q. Huang, Y. P. Lu, and Y. Nan, "A survey of numerical algorithms for trajectory optimization of flight vehicles," *SCIENCE CHINA Technological Sciences*, vol. 55, no. 9, pp. 2538–2560, 2012.